Journal of Materials Chemistry A

ROYAL SOCIETY OF CHEMISTRY

PAPER

View Article Online
View Journal | View Issue

Cite this: J. Mater. Chem. A, 2024, 12, 8429

Cutting off the upstream and downstream costs for CO_2 electroreduction by upcycling fermentation emissions into ethanol†

Ruofan Sun,‡[ab] Jiwu Zhao‡[ab] and Xu Lu *[ab]

Electrochemical reduction of CO_2 (CO_2RR), when powered by renewables, opens up a new avenue to mitigate the greenhouse gas while producing value sustainably. Nevertheless, this technology has been largely limited by the high costs of the upstream CO_2 feed and downstream product separation. Here we report a hybrid bio-electrochemical system, integrating yeast fermentation with CO_2RR in one single cell, that upcycles the fermentation-emitted CO_2 into ethanol. We engineer a CuO–Ag tandem electrocatalyst with rationally designed CuO–Ag interfaces that pose minimal impact on the yeast, while efficiently converting CO_2 into ethanol against side reactions, such as hydrogen evolution and glucose reduction. We showcase the win–win model enabled by this hybrid system—the CO_2RR cost can be cut by 17.8% because the fermentation process provides a free, high-purity CO_2 source and free ethanol distillation and in return, the CO_2RR reduces the CO_2 emissions of fermentation and increases the final ethanol product concentration. This proof-of-concept procedure sheds light on a tempting possibility for a cost-effective CO_2 value chain.

Received 6th December 2023
Accepted 21st February 2024

DOI: 10.1039/d3ta07558c

rsc.li/materials-a

Xu Lu

Dr Xu Lu obtained his BS and PhD degrees from the Department of Mechanical Engineering, University of Hong Kong in 2012 and 2017, respectively. He was then trained as a postdoctoral fellow in the Energy Sciences Institute, Yale University. Dr Lu joined King Abdullah University of Science and Technology (KAUST) as an Assistant Professor in Mechanical Engineering in March 2021. He established the Low-carbon Energy Conversion and Storage (LECS) Laboratory, which focuses on electrochemical upcycling of industrial high-pressure CO_2. So far, the LECS Laboratory has published original research articles in Nature Communications (3), Journal of the American Chemical Society, Angewandte Chemie, Chemical Engineering Journal, Journal of Energy Chemistry, etc., and generated two US provisional patents. The LECS Laboratory is also developing kilowatt-scale electrolyzers with industrial partners such as ACWA Power and Saudi Aramco.

Introduction

Renewable-driven production of value-added chemicals *via* electrochemical reduction of CO_2 (CO_2RR) holds promise to simultaneously benefit environmental sustainability and realize a low carbon footprint in manufacturing industry.[1–3] To date, the field has demonstrated high-yield and efficient production of multiple CO_2RR products, including carbon monoxide (CO), formic acid/formate (HCOOH or $HCOO^-$), methane (CH_4), methanol (CH_3OH), ethylene (C_2H_4), acetic acid/acetate (CH_3COOH or CH_3COO^-), and ethanol (CH_3CH_2OH).[4–6] Converting CO_2 to ethanol is of particular importance because ethanol is a high-energy-density fuel additive that can facilitate cleaner combustion compared to conventional gasoline, such as the E85 ethanol fuel.[7–9] Ethanol also serves as the key chemical in pharmaceutical and cosmetic industries.[10,11] According to a report by GlobeNewswire, ethanol consumption in the European Union was estimated at approximately 4.8 million tons in 2021.[12]

Despite major advances, CO_2RR technology has been greatly challenged by its costly upstream and downstream processes.[13–15] On the one hand, the upstream feed of CO_2RR should be high-purity CO_2, due to the substantial energy and capital expenses required for direct electroreduction of impure

[a]CCRC, Division of Physical Science and Engineering (PSE), King Abdullah University of Science and Technology (KAUST), Thuwal, 23955-6900, Kingdom of Saudi Arabia. E-mail: xu.lu@kaust.edu.sa

[b]KAUST Solar Center (KSC), PSE, KAUST, Kingdom of Saudi Arabia

† Electronic supplementary information (ESI) available. See DOI: https://doi.org/10.1039/d3ta07558c

‡ These authors contributed equally.

CO_2.[16–18] The prevailing way to generate pure CO_2 gas is to capture CO_2 from point sources or air. Recent studies have described the possibility of integrating CO_2 capture with CO_2RR.[19–21] However, for now at least, CO_2 capture and recycling still incurs a high cost, which accounts to 9.3% of the capital expenditure (CapEx) and 8.3% of the operating expense (OpEx).[22–24] On the other hand, residue CO_2 and the electrolyte solution hold a large portion of the CO_2RR effluent, and this necessitates downstream separation of products, which is another constraint of CO_2RR. Taking ethanol as an example again, the commonly used distillation apparatus not only leads to significant energy compensation, but also jeopardizes the cost effectiveness of the process—contributing approximately 3.9% CapEx and 2.3% OpEx of the overall CO_2RR process.[13,24,25]

Bio-ethanol, produced from biomass through yeast fermentation, is the world's most popular ethanol supply, with a market size of $46.18 billion in 2022.[26,27] However, a typical bio-fermentation process produces bio-ethanol *via* reaction in an anaerobic environment:

$$C_6H_{12}O_6 \xrightarrow{\text{Yeast}} 2CO_2 + 2C_2H_5OH \quad (1)$$

where significant amounts of CO_2 are emitted as a side product.[28] Different from fermentation in an aerobic reaction environment, where oxygen plays a part as a gas reactant, the emitted CO_2 in bio-ethanol fermentation has been proposed for use in food industry applications as a result of its high purity.[29] The global bio-ethanol yield in 2022 was 140 billion liters.[30] That means that approximately 106 million tons of CO_2 were emitted, leading to adverse environmental impacts and a heavy carbon penalty. It is estimated that the bio-ethanol manufacturing industry has been investing over $1.67–3.32 billion per year on the treatment of fermentation emissions.[31] However, fermentation CO_2 emission exhibits ultra-high purity (Fig. 1a),[32] and is thereby a perfect CO_2RR input feed. Meanwhile, CO_2 from ambient air or other point sources, such as vehicle exhaust, oil refineries, steam reforming, ammonia production, iron and steel casting, and cement manufacture, usually come with significant amounts of impurities. In addition, the fermentation process consists of an ethanol distillation step, which could well serve the purpose of product separation for CO_2RR, if carefully designed.

Here we propose a fermentation–CO_2RR hybrid that electrochemically converts high-purity fermentation-generated CO_2 into ethanol, which is then distilled together with the fermentation-produced bio-ethanol without extra cost. We tailor a CuO–Ag tandem catalyst with CuO–Ag interfaces that pose minimal influence on yeast activity while maintaining a reasonable faradaic efficiency (FE) for CO_2-to-ethanol conversion. *In situ* Raman studies show that the role of the CO intermediate on the CuO–Ag surface accelerates the C–C coupling process, reversibly suppressing side reactions such as hydrogen evolution and glucose reduction. Techno-economic analysis (TEA) indicates that our system not only cuts off the upstream and downstream expenses of CO_2RR (that is, around 17.8% of the total CO_2RR cost), but also benefits the fermentation by reducing CO_2 emissions. This proof-of-concept system provides the possibility to address major bottlenecks for both CO_2RR and fermentation.

Results

Pathway design

CO_2RR suffers from high costs of the (i) upstream CO_2 feed and (ii) downstream product separation, making it challenging for commercialization. We therefore propose a fermentation–CO_2RR hybrid for CO_2RR to take a free ride on the bio-fermentation process, which affords the possibility of cutting the two major costs of CO_2RR, by supplying high-purity CO_2 and providing free ethanol distillation. The proposed bio-electrochemical system (Fig. 1b) realizes a greener production of ethanol *via* a three-step pathway as below.

(i) Biomass fermentation as catalyzed by yeast, where ethanol is generated with high-purity CO_2 emission:

$$C_6H_{12}O_6 \xrightarrow{\text{Yeast}} 2CO_2 + 2C_2H_5OH; \quad (2)$$

(ii) CO_2RR powered by renewables, where the CO_2 emission is upcycled into ethanol:

$$2CO_2 + 12H^+ + 12e^- \xrightarrow{\text{Green electricity}} C_2H_5OH + 3H_2O; \quad (3)$$

(iii) Ethanol distillation for the delivery of final product.

To confirm the cost effectiveness of the fermentation–CO_2RR hybrid system, we performed TEA for CO_2 electroreduction to ethanol, assuming a base electricity cost of 0.02 $ per kW h, in line with the target set by US Department of Energy (DOE) for the year 2030.[33] TEA revealed that the CO_2 feed and the ethanol distillation accounted for 9.1% and 8.7% of the total CO_2RR cost with an operating current density of 200 mA cm^{-2} and ethanol FE of 50%—that is, 17.8% of the expense can be saved by our proposed system compared to a stand-alone CO_2RR device (Fig. 1c).

To realize this proof-of-concept system, we first need to validate the CO_2 output from fermentation. We used 0.1 M glucose solution, as is commonly used in literature, as the fermentation feedstock for yeast to generate ethanol.[34,35] Despite the fact that liquids such as glycerol and organic acids may exist as side products, CO_2 was the only gas product from anaerobic bio-ethanol fermentation, as analyzed by gas chromatography (GC)—that is, almost 100% CO_2 purity (Fig. 2a).[36] After 25 h of fermentation, CO_2 became saturated, and the saturation state lasted for at least 500 h (Fig. 2b). This indicated the capability of the fermentation to supply sufficient CO_2 to CO_2RR over a prolonged time. The pH value of the fermentation broth remained stable at 5.83 (Fig. 2c), which provides a weakly acidic environment that is beneficial to a high-carbon utilization efficiency during CO_2RR because the otherwise neutral or alkaline environment at the cathode–electrolyte interface may lead to carbonate formation.[37–39] These observations authenticated the idea of feeding the fermentation CO_2 emissions to the CO_2RR, and motivated us to conduct the subsequent electrochemical experiments.

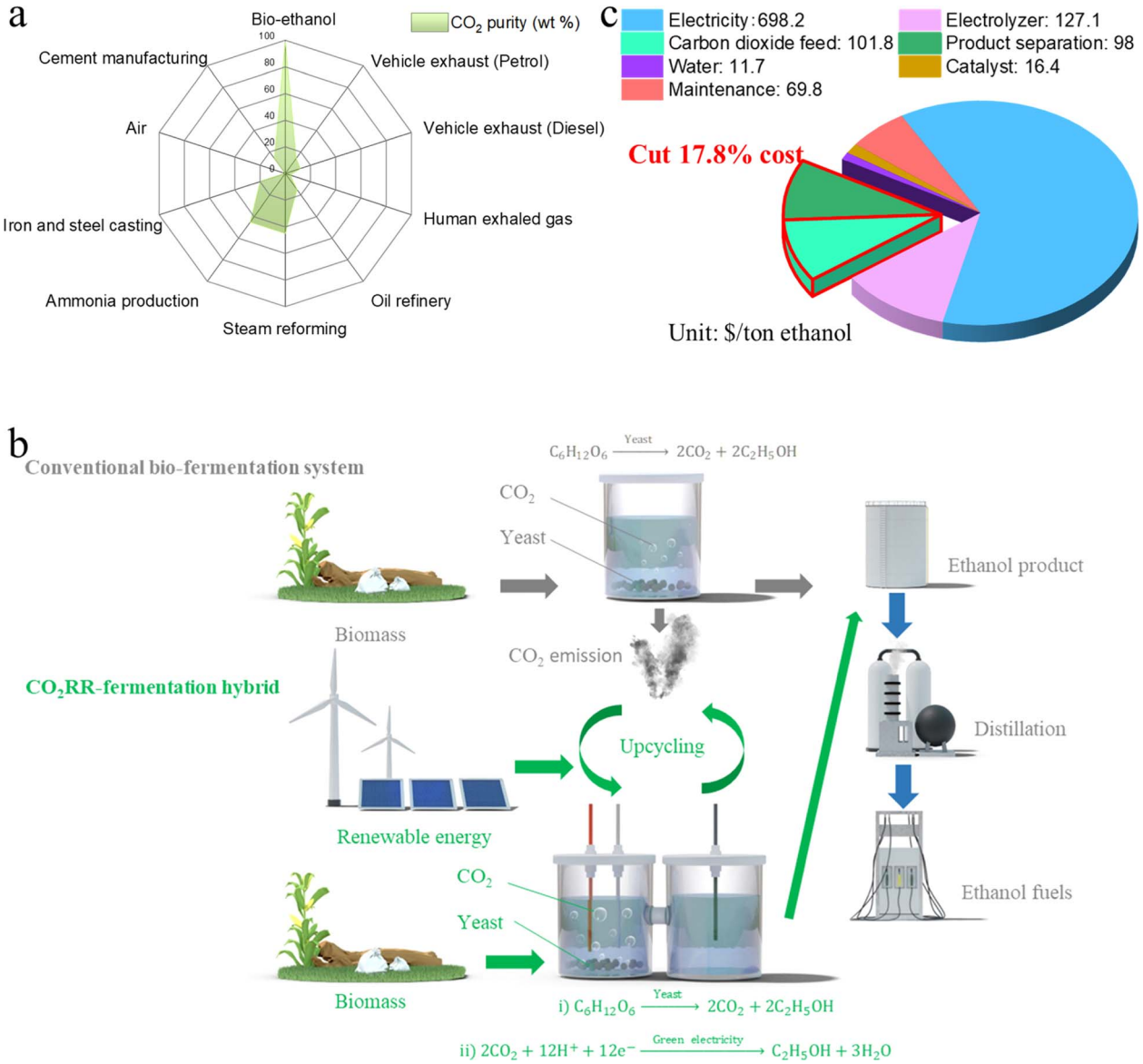

Fig. 1 Schematics of TEA and the proposed hybrid system. (a) CO_2 purity (wt%) of various point sources and ambient air. (b) Schematic illustration of the fermentation–CO_2RR hybrid system. Bio-fermentation emits CO_2, which is upcycled into ethanol *via in situ* electrochemical conversion. This ethanol produced by the CO_2RR is then distilled together with the fermentation-generated bio-ethanol without extra cost. (c) Techno-economic analysis (TEA) of the proposed bio-electrochemical system *vs.* the conventional CO_2RR process for the production of ethanol. Our system saves on the costs of (i) acquiring high-purity CO_2 feed and (ii) separating the final product, thereby cutting the CO_2RR cost by at least 17.8%.

CuO–Ag tandem catalyst for the fermentation–CO_2RR hybrid

Catalyst design strategies for CO_2RR to ethanol have been extensively studied, such as surface control, oxide modulation, oxophilicity engineering, *etc.*[40–42] Recently, tandem catalysts, especially Cu–Ag tandems, have demonstrated the capability of sequentially catalyzing CO_2-to-CO and CO-to-C_2 at reaction rates approaching industrial relevance.[43,44] Other homogeneously alloyed Cu-based bimetallic nanoparticles, as well as segmented tandem electrodes for increased CO coverage, can also enhance the CO_2-to-ethanol conversion.[45,46] For instance, CoPc@HC/Cu tandem electrode in acid CO_2RR exhibited a C_{2+} FE of 90% and single-pass CO_2 conversion efficiency of 76%.[47] We therefore sought to explore the possibility of designing a CuO–Ag tandem catalyst for our system (Fig. 3a). In brief, an Ag layer was first deposited on a carbon paper, followed by shadow mask-based Cu deposition to create 40 CuO–Ag interfaces in a 0.5 cm × 2 cm area. Of note, interface numbers higher than 40 were not prepared due to instrumentation constraints. Then, the electrode underwent galvanostatic anodic oxidation to form the final CuO–Ag tandem (Fig. 3b and S1†). The CuO–Ag interfaces were confirmed by transmission electron microscopy (TEM), electron energy loss spectroscopy (EELS), and energy-dispersive spectroscopy (EDS). Cu(111) and Ag(111) facets were delineated (Fig. 3c). EELS revealed the interface structure

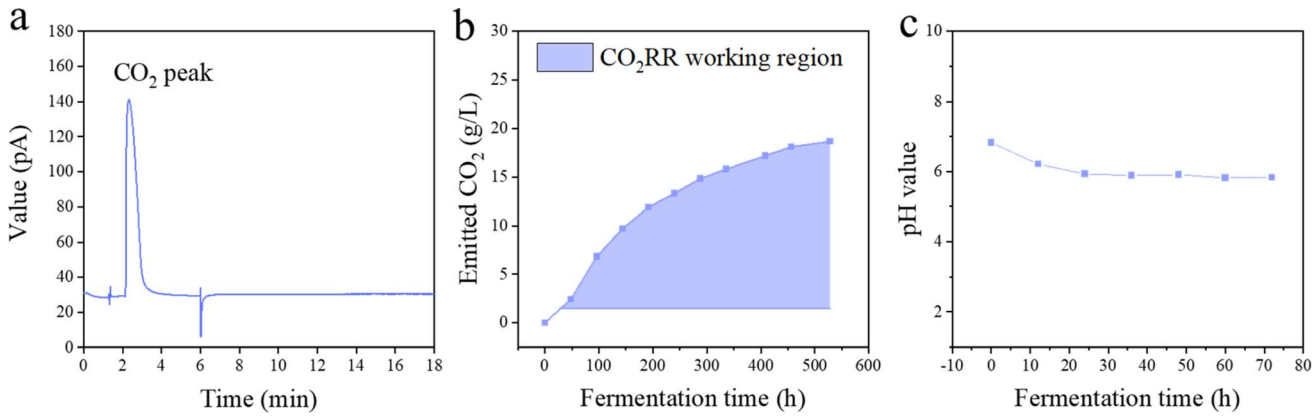

Fig. 2 Fermentation emissions and broth condition. (a) Gas chromatography of fermentation-emitted CO_2. CO_2 is the only gas product. (b) Amount of fermentation-emitted CO_2 and (c) pH value of the fermentation broth over time.

at the nanoscale (Fig. 3d), while EDS uncovered the CuO–Ag at microscale (Fig. S2†). X-ray diffraction (XRD) patterns of the Cu segment of the as-prepared tandem electrode showed that CuO(110), CuO(111), and CuO (022) peaks increased during electrochemical oxidation, while those of Cu(111) and Cu(200) decreased over time (Fig. 3e), which implies the formation of CuO.[48] This was confirmed using Raman spectroscopy, which showed the characteristic peaks of CuO at 282, 330, and 616 cm^{-1}. Consistent with the literature, CuO exhibited a nanoplate morphology, while Ag appeared as nanoparticles (Fig. 3g and S3†).[49]

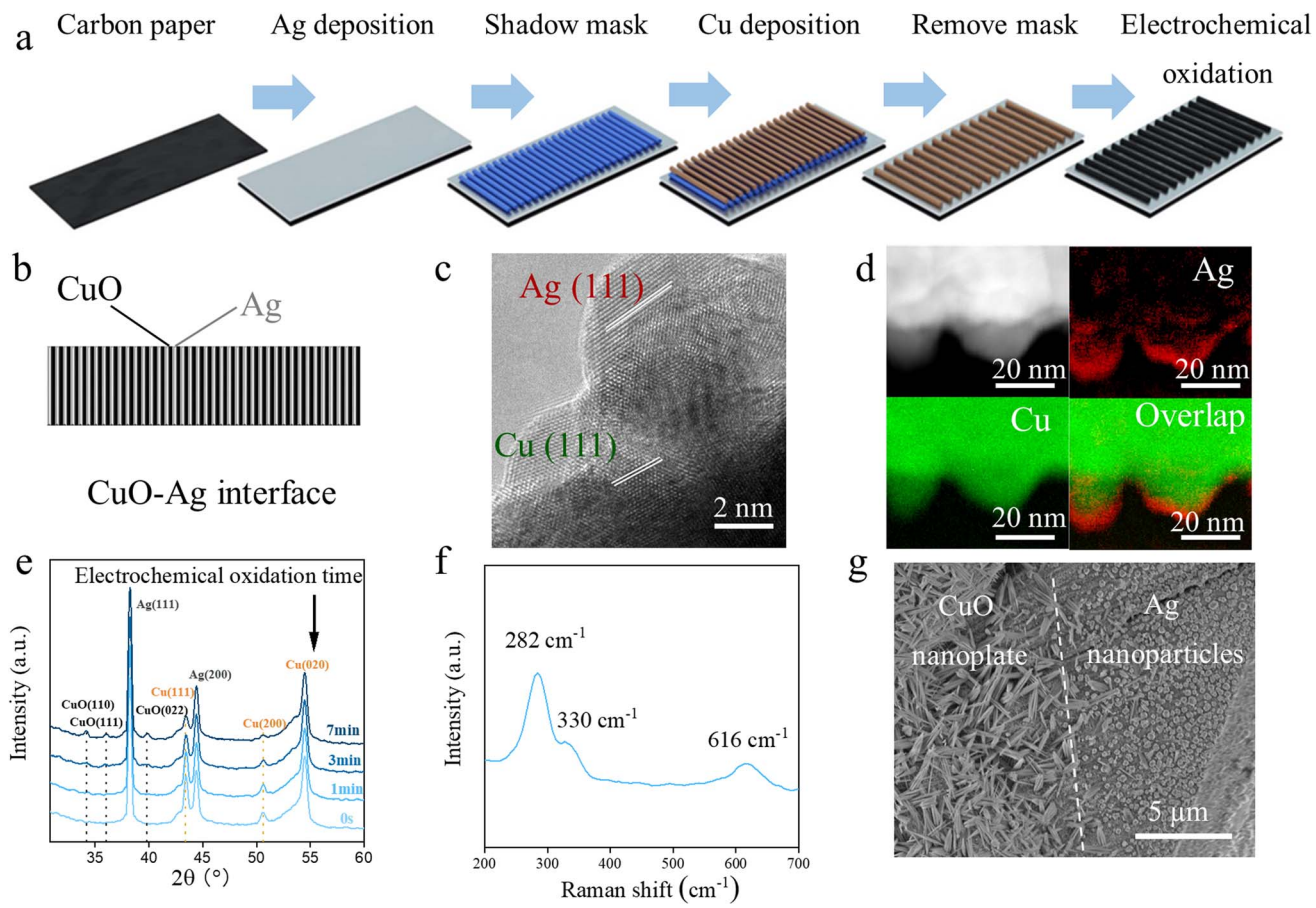

Fig. 3 CuO–Ag tandem catalyst. Schematic of (a) the CuO–Ag tandem electrode synthesis and (b) the CuO–Ag interfaces. (c) HR-TEM and (d) EELS elemental mapping of the CuO–Ag interface. (e) XRD patterns of CuO–Ag over the electrochemical oxidation time. (f) Raman spectroscopy and (g) SEM of the CuO segment after oxidation.

We then retrofitted a conventional fermentation system into an H-type hybrid cell that is compatible with CO_2RR—the cathode compartment contained 0.1 M glucose (a typical fermentation broth) and the anode compartment was filled with 0.5 M $KHCO_3$ aqueous solution (Fig. 4a). Nevertheless, the fermentation broth cannot provide the necessary electrochemical reaction conditions—the low electrolyte concentration resulted in sluggish adsorption of OH^- on the catalyst surface, and increased both the charge transfer resistance (R_{ct}) and the electrical double layer (EDL) thickness.[50,51] Consequently, the CO_2RR current density was limited below 8.85 mA cm^{-2} at cathode potentials as negative as −1.6 V *vs.* the reversible hydrogen electrode (RHE) (Fig. 4b). To accommodate a reasonably high CO_2RR reactivity, we attempted to add the most used cation, K^+, into the fermentation broth, such as K_2CO_3, KCl, and $KHCO_3$.[52–54] At a cathode potential of −1.6 V *vs.* RHE, the current density reached −181, −152, and −161 mA cm^{-2} in 0.5 M K_2CO_3, 0.5 M KCl, and 0.5 M $KHCO_3$ glucose solutions, respectively, which is significantly higher than those in 0.1 M glucose, as suggested by linear sweep voltammetry (LSV) curves (Fig. 4b). However, the addition of carbonate and bicarbonate anions resulted in an adverse impact on fermentation by tuning the pH towards alkaline, which was unfavorable for yeast activity,[55] whereas adding KCl maintained the fermentation broth as a weak acid to facilitate the fermentation process (Fig. S4†).[56] This was further confirmed by weighing the fermentation CO_2 emissions, where 0.5 M KCl merely changed the amount of yeast-generated CO_2, while in the case of K_2CO_3 and $KHCO_3$ obvious degradation of yeast activity was shown (Fig. 4c).[57] Therefore, we selected 0.1 M glucose aqueous solution (0.5 M KCl) as the catholyte for the fermentation–CO_2RR hybrid cell.

Rationally, more CuO–Ag interfaces in a fixed area should benefit the CO_2-to-CO and CO-to-ethanol tandem reaction.[58,59] To confirm this, we compared CuO–Ag interface numbers of 0 (*i.e.* CuO), 10, 20, 30, and 40. It was observed that increasing the interface number resulted in higher ethanol selectivity; at −0.87 V *vs.* RHE, the ethanol FE was improved from 14.4% on CuO to 27.7% on CuO–Ag (20), and eventually reached 42.7% on CuO–Ag (40). Similar phenomena hold for the ethanol

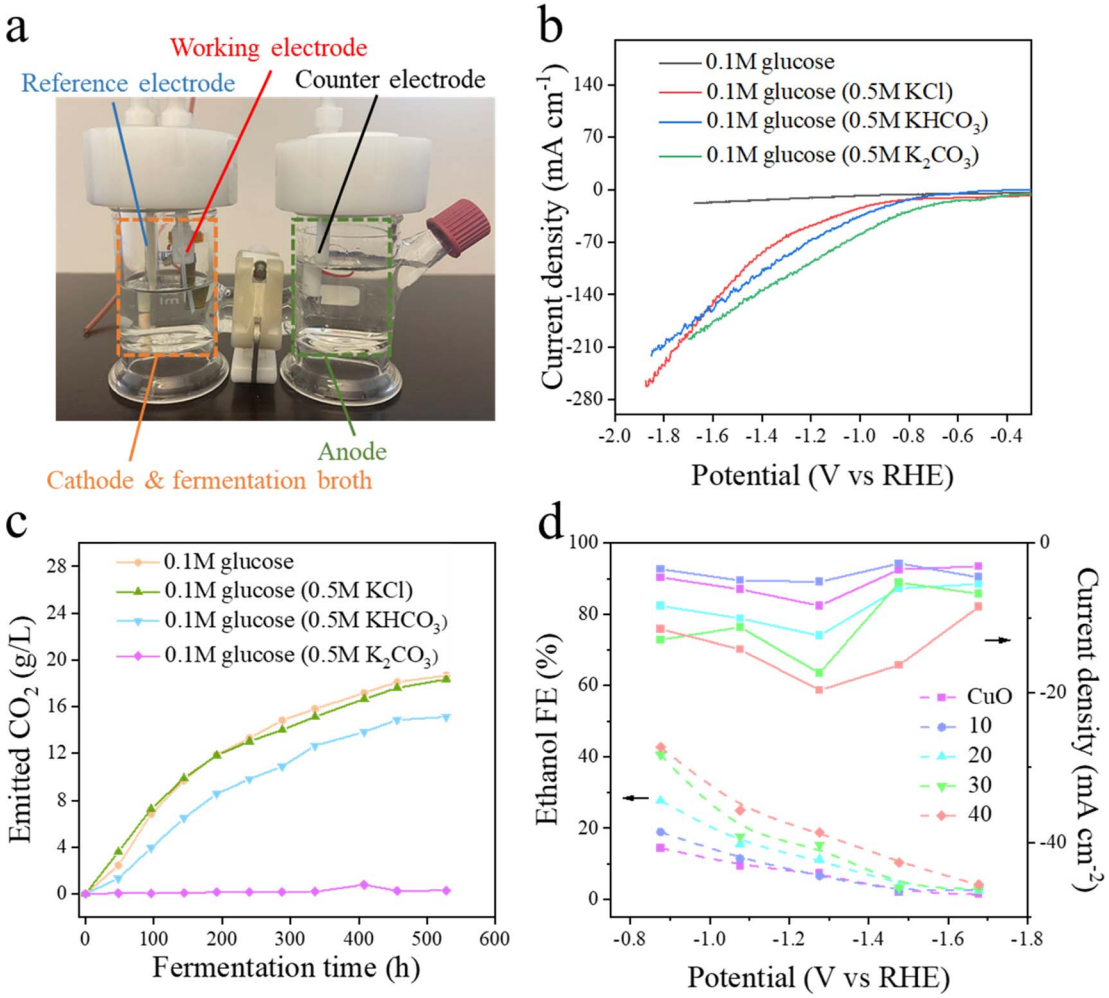

Fig. 4 CO_2RR performance in the fermentation–CO_2RR hybrid cell. (a) Photo of the fermentation–CO_2RR hybrid cell. (b) LSV curves of the CuO–Ag catalyst in different solutions. (c) Amount of fermentation CO_2 emissions in various glucose solutions. (d) Ethanol FEs and partial current densities with different CuO–Ag interface numbers (0, 10, 20, 30, and 40) in 0.1 M glucose (0.5 M KCl).

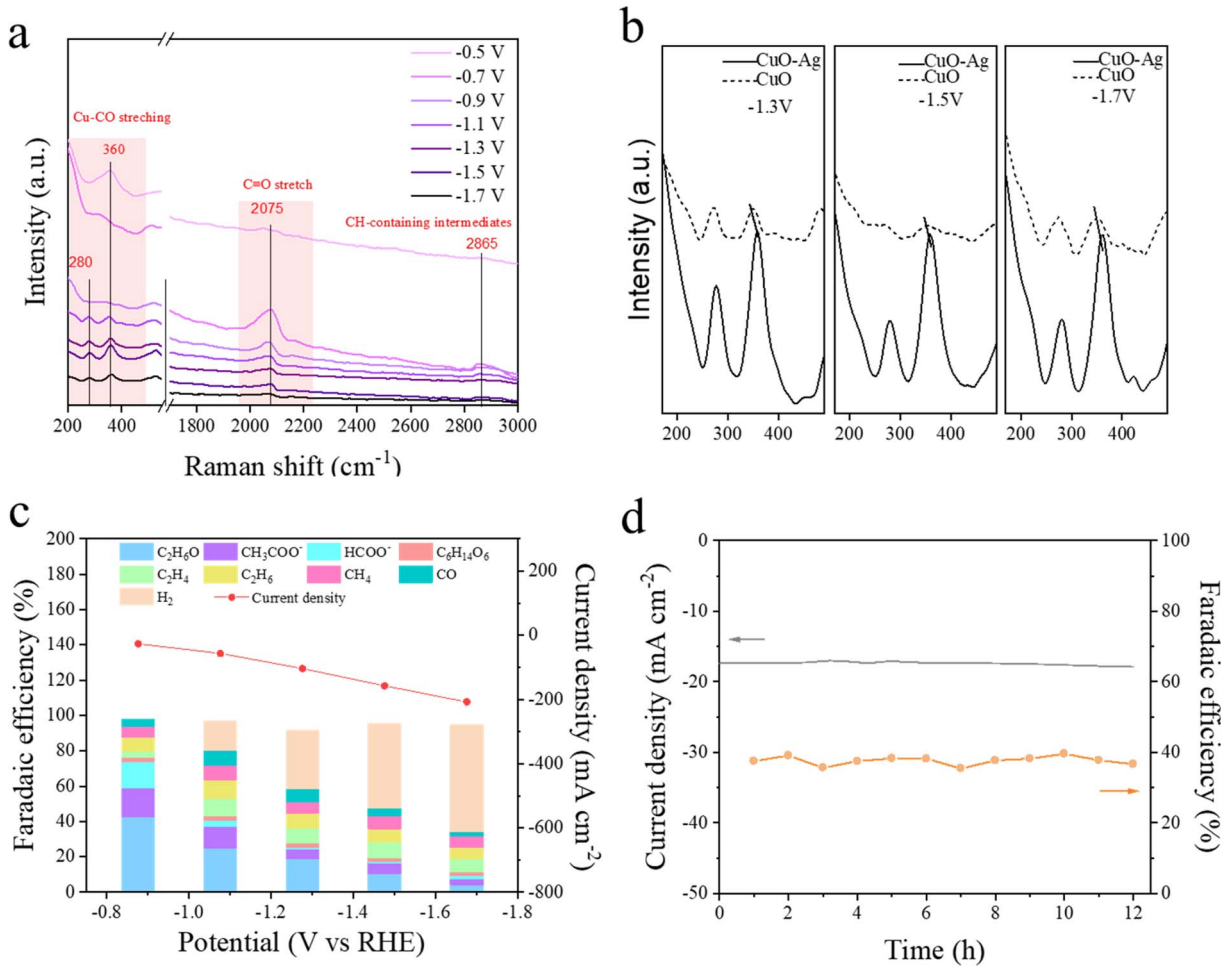

Fig. 5 Enhanced ethanol production and proof-of-concept demonstration. (a) *In situ* Raman spectra acquired on CuO–Ag (40) under different potentials. (b) Comparison of *in situ* Raman spectra on CuO–Ag (40) and CuO catalysts at −1.3, −1.5, and −1.7 V *vs.* RHE. (c) FEs and current densities toward CO_2RR products, H_2, and sorbitol. (d) Prolonged operation of the CO_2RR–fermentation hybrid at −0.87 V *vs.* RHE. Pt foil was used as the anode. 0.1 M glucose (0.5 M KCl) solution was the electrolyte, and the CuO–Ag interface number was 40 unless otherwise stated.

productivity; at −1.27 V *vs.* RHE, the partial current density of ethanol was −8.4 mA cm^{-2} on CuO, whereas it gradually increased to −19.6 mA cm^{-2} on CuO–Ag (40) under the same conditions (Fig. 4d).

Understanding the enhanced ethanol production for proof-of-concept

To gain insights into the improved ethanol yield at higher CuO–Ag interface numbers, *in situ* studies and density functional theory (DFT) calculations were conducted. Time-resolved X-ray diffractograms (Fig. S5†) revealed that CuO was reduced to Cu(111) and Cu(200) under CO_2RR condition, whereas the diffraction peaks of Ag barely changed, which is consistent with the X-ray photoelectron spectroscopy (XPS) results (Fig. S6†). This indicated that metallic Cu and Ag served as the dominant active sites during electrolysis, and prepared us to probe the key species distributions on the catalyst surface using *in situ* Raman spectroscopy. As mentioned above, the conversion of CO_2 to ethanol on a tandem catalyst proceeded *via* two steps: (i) CO formation, as catalyzed by Ag (Fig. S7 and S8†) and (ii) C–C coupling, as catalyzed by Cu. Three regions in the Raman spectra were associated with the CO intermediates on the surface at negative potentials—the band at around 280 cm^{-1} referred to the Cu–CO frustrated rotation mode,[58,60,61] the band at 360 cm^{-1} was related to the Cu–CO stretch mode,[60,62] and the band at approximately 2075 cm^{-1} can be ascribed to the C≡O stretch of the top-bound CO (Fig. 5a).[63,64] Compared to CuO, the band of the Cu–CO stretch was blue-shifted on the CuO–Ag interface at −1.3, −1.5, and −1.7 V *vs.* RHE (Fig. 5b and S9†), indicating a stronger binding of CO to the CuO–Ag interface.[65–67] The enhanced CO binding implied an enriched CO environment, which would promote the subsequent C–C coupling step, thereby resulting in a higher ethanol productivity.[68] DFT calculations confirm that the interface of Cu–Ag is more effective in ethanol generation (Fig. S10†). Compared to bare Cu, the free energy difference on the Cu–Ag interface is more gradual. For instance, the energy difference for adsorption of the second CO_2 is lower on the Cu–Ag interface (0.27 eV *vs.* 0.79 eV). Additionally, for C–C coupling, the Cu–Ag interface exhibits lower energy (1.09 eV *vs.* 1.46 eV).

To further rationalize our choice of a high CuO–Ag interface number, we examined the side reactions that occurred simultaneously with CO_2RR. In a typical CO_2RR cell, the hydrogen evolution reaction (HER) is known to be the major competing reaction,[69–73] and it was slightly impacted by the CuO–Ag interface number because the active sites for the HER were essentially unchanged. In our CO_2RR–fermentation hybrid system, however, another competing reaction existed, namely, the glucose reduction reaction (GRR), where glucose is electrochemically reduced to sorbitol.[74] Compared to the HER, the GRR may pose a greater threat to CO_2RR because both Cu and Ag have been reported to be active GRR catalysts.[75] Strikingly, our CuO–Ag (40) catalyst can effectively suppress the GRR: the GRR FE was 2.68% at −1.27 V *vs.* RHE, and this number even lower at 2.37% at −0.87 V *vs.* RHE (Fig. 5c). By stark contrast, the GRR FE increased to 2.91%, 3.51%, 3.71%, and 4.86% when the CuO–Ag interface number was 30, 20, 10, and 0, respectively (Fig. S11†). These observations verified our tandem catalyst design strategy, and, to the best of our knowledge, developing a CO_2RR catalyst that can simultaneously suppress the GRR has never been reported. Finally, we sought to stably operate the proof-of-concept system. Our CO_2RR–fermentation hybrid exhibited a maximal ethanol FE of 42.7% at −0.87 V *vs.* RHE, with an overall current density of 27 mA cm^{-2} (Fig. 5c). The partial current density towards ethanol reached 20 mA cm^{-2}, with an FE of 18.9% at −1.27 V *vs.* RHE. The current density and ethanol FE were well retained over the course of 12 h of chronoamperometric operation at −0.87 V *vs.* RHE (Fig. 5d). Ethanol was detected as the predominant liquid product (Fig. S12†).

Conclusions

In summary, we have demonstrated a compelling bioelectrochemical system, combining yeast fermentation and CO_2RR, to upcycle the fermentation-emitted CO_2 into ethanol. Taking a free ride from the high-purity CO_2 emissions and ethanol distillation during fermentation, the CO_2RR–fermentation hybrid cuts the total CO_2RR cost by 17.8%. A CuO–Ag tandem electrocatalyst with minimal impact on yeast was rationally designed, efficiently converting CO_2 to ethanol while suppressing side reactions, such as hydrogen evolution and glucose reduction. These results illustrate the possibility of a cost-effective CO_2 value chain for ethanol production. Further improvements are expected by optimizing the ethanol efficiency and yield through rational tandem electrode design, yeast selection, and system integration.

Author contributions

X. L. supervised the project. X. L. and R. S. conceived the idea. R. S. synthesized and characterized the catalysts, and conducted electrochemical measurements. J. Z. made the DFT calculations. R. S. performed the fermentation experiments. R. S. and J. Z. carried out *in situ* Raman spectroscopy. R. S. conducted the TEA calculation. R. S. and X. L. wrote the manuscript. All authors discussed the results and assisted with the manuscript preparation.

Conflicts of interest

The authors declare no competing interests.

Acknowledgements

This work was financially supported by the Baseline Fund (BAS/1/1413-01-01) to X. L. from King Abdullah University of Science and Technology (KAUST).

References

1 O. S. Bushuyev, P. De Luna, C. T. Dinh, L. Tao, G. Saur, J. van de Lagemaat, S. O. Kelley and E. H. Sargent, *Joule*, 2018, **2**, 825–832.
2 Y. Wu, Z. Jiang, X. Lu, Y. Liang and H. Wang, *Nature*, 2019, **575**, 639–642.
3 R. G. Grim, Z. Huang, M. T. Guarnieri, J. R. Ferrell, L. Tao and J. A. Schaidle, *Energy Environ. Sci.*, 2020, **13**, 472–494.
4 G. Wang, J. Chen, Y. Ding, P. Cai, L. Yi, Y. Li, C. Tu, Y. Hou, Z. Wen and L. Dai, *Chem. Soc. Rev.*, 2021, **50**, 4993–5061.
5 W. Ma, X. He, W. Wang, S. Xie, Q. Zhang and Y. Wang, *Chem. Soc. Rev.*, 2021, **50**, 12897–12914.
6 D. Gao, R. M. Arán-Ais, H. S. Jeon and B. Roldan Cuenya, *Nat. Catal.*, 2019, **2**, 198–210.
7 A. Salvo and F. M. Geiger, *Nat. Geosci.*, 2014, **7**, 450–458.
8 P. Zhu and H. Wang, *Nat. Catal.*, 2021, **4**, 943–951.
9 C. E. Wyman and N. D. Hinman, *Appl. Biochem. Biotechnol.*, 1990, **24**, 735–753.
10 A. Duereh, H. Guo, T. Honma, Y. Hiraga, Y. Sato, R. Lee Smith Jr and H. Inomata, *Ind. Eng. Chem. Res.*, 2018, **57**, 7331–7344.
11 D. W. Lachenmeier, *J. Occup. Med. Toxicol.*, 2008, **3**, 1–16.
12 *EU Ethanol Market Report: Suppliers, Prices, Trends and Forecast to 2030*, IndexBox, 2022.
13 M. Jouny, W. Luc and F. Jiao, *Ind. Eng. Chem. Res.*, 2018, **57**, 2165–2177.
14 M. G. Kibria, J. P. Edwards, C. M. Gabardo, C. T. Dinh, A. Seifitokaldani, D. Sinton and E. H. Sargent, *Adv. Mater.*, 2019, **31**, 1807166.
15 J. M. Spurgeon and B. Kumar, *Energy Environ. Sci.*, 2018, **11**, 1536–1551.
16 P. Li, X. Lu, Z. Wu, Y. Wu, R. Malpass-Evans, N. B. McKeown, X. Sun and H. Wang, *Angew. Chem., Int. Ed.*, 2020, **59**, 10918–10923.
17 X. Lu, Z. Jiang, X. Yuan, Y. Wu, R. Malpass-Evans, Y. Zhong, Y. Liang, N. B. McKeown and H. Wang, *Sci. Bull.*, 2019, **64**, 1890–1895.
18 Y. Xu, J. P. Edwards, J. Zhong, C. P. O'Brien, C. M. Gabardo, C. McCallum, J. Li, C.-T. Dinh, E. H. Sargent and D. Sinton, *Energy Environ. Sci.*, 2020, **13**, 554–561.
19 G. Lee, A. S. Rasouli, B.-H. Lee, J. Zhang, Y. C. Xiao, J. P. Edwards, M. G. Lee, E. D. Jung, F. Arabyarmohammadi, H. Liu and E. Sargent, *Joule*, 2023, **7**, 1277–1288.
20 Y. Cheng, J. Hou and P. Kang, *ACS Energy Lett.*, 2021, **6**, 3352–3358.

21 A. J. Welch, E. Dunn, J. S. DuChene and H. A. Atwater, *ACS Energy Lett.*, 2020, **5**, 940–945.
22 M. T. Ho, G. W. Allinson and D. E. Wiley, *Energy Procedia*, 2009, **1**, 763–770.
23 A. Raksajati, M. T. Ho and D. E. Wiley, *Ind. Eng. Chem. Res.*, 2013, **52**, 16887–16901.
24 M. Ramdin, B. De Mot, A. R. Morrison, T. Breugelmans, L. J. Van Den Broeke, J. M. Trusler, R. Kortlever, W. De Jong, O. A. Moultos and P. Xiao, *Ind. Eng. Chem. Res.*, 2021, **60**, 17862–17880.
25 D. R. Sánchez, K. Khalilpour and A. F. Hoadley, *Sustainable Energy Fuels*, 2021, **5**, 5866–5880.
26 *Bioethanol Market (By Application: Transportation, Alcoholic Beverages, Cosmetics, Pharmaceuticals, Others; By Feedstock: Starch Based, Sugar Based, Cellulose-Based; By Fuel Generation: First Generation, Second Generation, Third Generation; By Blend: E5, E10, E15 to E70, E75 & E85, Others (E85 to E100)) – Global Industry Analysis, Size, Share, Growth, Trends, Regional Outlook, and Forecast 2022–2030, Report 2210*, Precedence Research, 2022.
27 *Ethanol fuel*, can be found under **https://en.wikipedia.org/wiki/Ethanol_fuel**, accessed April 2023.
28 F. Rodrigues, P. Ludovico and C. Leão, *Biodiversity and Eecophysiology of Yeasts*, 2006, pp. 101–121.
29 Q. Zhang, C.-L. Cheng, D. Nagarajan, J.-S. Chang, J. Hu and D.-J. Lee, *Appl. Energy*, 2017, **206**, 364–371.
30 I. Edeh, *Bioethanol Technologies*, 2021, p. 1.
31 J. K. Stolaroff, S. H. Pang, W. Li, W. G. Kirkendall, H. M. Goldstein, R. D. Aines and S. E. Baker, *Front. Energy Res.*, 2021, **9**, 639943.
32 H. Pilorgé, N. McQueen, D. Maynard, P. Psarras, J. He, T. Rufael and J. Wilcox, *Environ. Sci. Technol.*, 2020, **54**, 7524–7532.
33 DOE, can be found under **https://www.energy.gov/eere/solar/sunshot-2030**, accessed: October 2018.
34 A. F. Duro and R. Serrano, *Curr. Microbiol.*, 1981, **6**, 111–113.
35 A. Aminian and E. Motamedian, *Sci. Rep.*, 2023, **13**, 1165.
36 B. Maiorella, H. W. Blanch and C. R. Wilke, *Biotechnol. Bioeng.*, 1983, **25**, 103–121.
37 A. S. Varela, *Curr. Opin. Green Sustainable Chem.*, 2020, **26**, 100371.
38 J. A. Rabinowitz and M. W. Kanan, *Nat. Commun.*, 2020, **11**, 5231.
39 Y. Wu, K. Kamiya, T. Hashimoto, R. Sugimoto, T. Harada, K. Fujii and S. Nakanishi, *Electrochemistry*, 2020, **88**, 359–364.
40 Y. Zhao, L. Hao, A. Ozden, S. Liu, R. K. Miao, P. Ou, T. Alkayyali, S. Zhang, J. Ning, Y. Liang, Y. Xu, M. Fan, Y. Chen, J. E. Huang, K. Xie, J. Zhang, C. P. O'Brien, F. Li, E. H. Sargent and D. Sinton, *Nat. Synth.*, 2023, **2**, 403–412.
41 J. Li, A. Ozden, M. Wan, Y. Hu, F. Li, Y. Wang, R. R. Zamani, D. Ren, Z. Wang, Y. Xu, D.-H. Nam, J. Wicks, B. Chen, X. Wang, M. Luo, M. Graetzel, F. Che, E. H. Sargent and D. Sinton, *Nat. Commun.*, 2021, **12**, 2808.
42 M. Li, N. Song, W. Luo, J. Chen, W. Jiang and J. Yang, *Adv. Sci.*, 2023, **10**, 2204579.
43 P.-C. Chen, C. Chen, Y. Yang, A. L. Maulana, J. Jin, J. Feijoo and P. Yang, *J. Am. Chem. Soc.*, 2023, **145**, 10116–10125.
44 D. Wei, Y. Wang, C. L. Dong, Z. Zhang, X. Wang, Y. C. Huang, Y. Shi, X. Zhao, J. Wang and R. Long, *Angew. Chem.*, 2023, **135**, e202217369.
45 T. Zhang, J. C. Bui, Z. Li, A. T. Bell, A. Z. Weber and J. Wu, *Nat. Catal.*, 2022, **5**, 202–211.
46 L. Fan, C. Xia, F. Yang, J. Wang, H. Wang and Y. Lu, *Sci. Adv.*, 2020, **6**, eaay3111.
47 Y. Chen, X.-Y. Li, Z. Chen, A. Ozden, J. E. Huang, P. Ou, J. Dong, J. Zhang, C. Tian, B.-H. Lee, X. Wang, S. Liu, Q. Qu, S. Wang, Y. Xu, R. K. Miao, Y. Zhao, Y. Liu, C. Qiu, J. Abed, H. Liu, H. Shin, D. Wang, Y. Li, D. Sinton and E. H. Sargent, *Nat. Nanotechnol.*, 2023, **1**, 8.
48 Q. Lei, L. Huang, J. Yin, B. Davaasuren, Y. Yuan, X. Dong, Z.-P. Wu, X. Wang, K. X. Yao, X. Lu and Y. Han, *Nat. Commun.*, 2022, **13**, 4857.
49 W. Liu, P. Zhai, A. Li, B. Wei, K. Si, Y. Wei, X. Wang, G. Zhu, Q. Chen and X. Gu, *Nat. Commun.*, 2022, **13**, 1877.
50 S. S. Bhargava, F. Proietto, D. Azmoodeh, E. R. Cofell, D. A. Henckel, S. Verma, C. J. Brooks, A. A. Gewirth and P. J. Kenis, *ChemElectroChem*, 2020, **7**, 2001–2011.
51 M. König, J. Vaes, E. Klemm and D. Pant, *iscience*, 2019, **19**, 135–160.
52 J.-J. Li and Z.-C. Zhang, *Rare Met.*, 2022, **41**, 723–725.
53 X. Zhang, J. Li, Y.-Y. Li, Y. Jung, Y. Kuang, G. Zhu, Y. Liang and H. Dai, *J. Am. Chem. Soc.*, 2021, **143**, 3245–3255.
54 A. B. Moss, S. Garg, M. Mirolo, C. A. G. Rodriguez, R. Ilvonen, I. Chorkendorff, J. Drnec and B. Seger, *Joule*, 2023, **7**, 350–365.
55 Y. Lin, W. Zhang, C. Li, K. Sakakibara, S. Tanaka and H. Kong, *Biomass Bioenergy*, 2012, **47**, 395–401.
56 H. Zentou, Z. Z. Abidin, M. Zouanti and D. Greetham, *Int. J. Appl. Eng. Res.*, 2017, **12**, 5202–5506.
57 I. Jood, J. W. Hoff and M. E. Setati, *World J. Microbiol. Biotechnol.*, 2017, **33**, 1–11.
58 J. Li, H. Xiong, X. Liu, D. Wu, D. Su, B. Xu and Q. Lu, *Nat. Commun.*, 2023, **14**, 698.
59 C. Chen, Y. Li, S. Yu, S. Louisia, J. Jin, M. Li, M. B. Ross and P. Yang, *Joule*, 2020, **4**, 1688–1699.
60 C. Chen, X. Yan, S. Liu, Y. Wu, Q. Wan, X. Sun, Q. Zhu, H. Liu, J. Ma and L. Zheng, *Angew. Chem.*, 2020, **132**, 16601–16606.
61 J. Gao, H. Zhang, X. Guo, J. Luo, S. M. Zakeeruddin, D. Ren and M. Grätzel, *J. Am. Chem. Soc.*, 2019, **141**, 18704–18714.
62 J. Li, A. Ozden, M. Wan, Y. Hu, F. Li, Y. Wang, R. R. Zamani, D. Ren, Z. Wang and Y. Xu, *Nat. Commun.*, 2021, **12**, 2808.
63 F. Li, A. Thevenon, A. Rosas-Hernández, Z. Wang, Y. Li, C. M. Gabardo, A. Ozden, C. T. Dinh, J. Li and Y. Wang, *Nature*, 2020, **577**, 509–513.
64 G. Zhang, Z.-J. Zhao, D. Cheng, H. Li, J. Yu, Q. Wang, H. Gao, J. Guo, H. Wang and G. A. Ozin, *Nat. Commun.*, 2021, **12**, 5745.
65 A. Fielicke, P. Gruene, G. Meijer and D. M. Rayner, *Surf. Sci.*, 2009, **603**, 1427–1433.
66 X. Wang, Z. Wang, F. P. García de Arquer, C.-T. Dinh, A. Ozden, Y. C. Li, D.-H. Nam, J. Li, Y.-S. Liu, J. Wicks,

Z. Chen, M. Chi, B. Chen, Y. Wang, J. Tam, J. Y. Howe, A. Proppe, P. Todorović, F. Li, T.-T. Zhuang, C. M. Gabardo, A. R. Kirmani, C. McCallum, S.-F. Hung, Y. Lum, M. Luo, Y. Min, A. Xu, C. P. O'Brien, B. Stephen, B. Sun, A. H. Ip, L. J. Richter, S. O. Kelley, D. Sinton and E. H. Sargent, *Nat. Energy*, 2020, **5**, 478–486.

67 C. Zhan, F. Dattila, C. Rettenmaier, A. Bergmann, S. Kühl, R. García-Muelas, N. r. López and B. R. Cuenya, *ACS Catal.*, 2021, **11**, 7694–7701.

68 R. B. Sandberg, J. H. Montoya, K. Chan and J. K. Nørskov, *Surf. Sci.*, 2016, **654**, 56–62.

69 A. Goyal, G. Marcandalli, V. A. Mints and M. T. Koper, *J. Am. Chem. Soc.*, 2020, **142**, 4154–4161.

70 X. Li, H. Zhang, Q. Hu, W. Zhou, J. Shao, X. Jiang, C. Feng, H. Yang and C. He, *Angew. Chem., Int. Ed.*, 2023, **62**, e202300478.

71 X. Li, C. Deng, Y. Kong, Q. Huo, L. Mi, J. Sun, J. Cao, J. Shao, X. Chen and W. Zhou, *Angew. Chem., Int. Ed.*, 2023, **62**, e202309732.

72 Q. Hu, K. Gao, X. Wang, H. Zheng, J. Cao, L. Mi, Q. Huo, H. Yang, J. Liu and C. He, *Nat. Commun.*, 2022, **13**, 3958.

73 C. Feng, M. Lv, J. Shao, H. Wu, W. Zhou, S. Qi, C. Deng, X. Chai, H. Yang and Q. Hu, *Adv. Mater.*, 2023, **35**, 2305598.

74 A. Bin Kassim, C. Rice and A. Kuhn, *J. Appl. Electrochem.*, 1981, **11**, 261–267.

75 Y. Kwon and M. T. Koper, *ChemSusChem*, 2013, **6**, 455–462.